AIDA-PUB-2015-011

AIDA

Advanced European Infrastructures for Detectors at Accelerators

Journal Publication

Operation of a GEM-TPC with pixel readout

Brezina, C (UBONN) *et al*

06 December 2012

The research leading to these results has received funding from the European Commission under the FP7 Research Infrastructures project AIDA, grant agreement no. 262025.

This work is part of AIDA Work Package **9: Advanced infrastructures for detector R&D**.

The electronic version of this AIDA Publication is available via the AIDA web site <http://cern.ch/aida> or on the CERN Document Server at the following URL: <http://cds.cern.ch/search?p=AIDA-PUB-2015-011>

Operation of a GEM-TPC With Pixel Readout

C. Brezina, K. Desch, J. Kaminski, M. Killenberg, and T. Krautscheid

***Abstract*—A prototype time projection chamber with 26 cm drift length was operated with a short-spaced triple gas electron multiplier (GEM) stack in a setup triggering on cosmic muon tracks. A small part of the anode plane is read out with a CMOS pixel application-specified integrated circuit (ASIC) named Timepix, which provides ultimate readout granularity. Pixel clusters of charge depositions corresponding to single primary electrons are observed and analyzed to reconstruct charged particle tracks. A dataset of several weeks of cosmic ray data is analyzed. The number of clusters per track length is well described by simulation. The obtained single point resolution approaches 50 μm at short drift distances and is well reproduced by a simple model of single-electron diffusion.**

***Index Terms*—Gas electron multiplier (GEM), International Linear Collider (ILC), medipix, micro pattern gaseous detector (MPGD), time projection chamber (TPC), Timepix.**

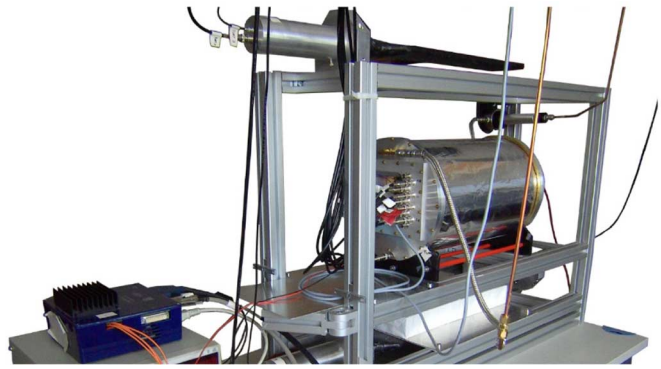

Fig. 1. Cosmic ray test stand. Scintillators for triggering are placed above and below the sensitive volume [15].

I. Introduction

TIME projection chambers (TPCs) [1] have been employed in numerous large-scale experiments for precise charged-particle tracking. In recent years, the suitability of novel gas amplification structures for TPCs, in particular micro pattern gaseous detectors (MPGDs), has been studied. For example, Micromegas [2] are in operation in the T2K neutrino experiment [3]. Gas electron multipliers (GEMs) [4] have been studied for several years as an amplification structure for the ILD concept [5] at the future International Linear Collider (ILC) [6]. Within the international LCTPC collaboration [7], various MPGD-based readout options are pursued. A common approach to achieve the ambitious resolution goal for an ILC detector of less than 100 μm at zero drift distance is to reduce the size of conventional readout pads down to a few millimeters squared (mm^2) and connect the pads to integrated readout chips on the back of the anode plane.

In this paper, an alternative approach is studied. In order to reach a granularity that matches that of the MPGD structures themselves, the anode plane may itself consist of pixelized CMOS readout application-specific integrated circuits (ASICs) to collect and amplify the deposited charge. In doing so, an unprecedented readout granularity of down to several tens of micrometers squared (μm^2) can be provided. This approach has first been pursued for X-ray polarimetry [8], [9]. Several studies have been performed using the Medipix [10] and Timepix [11] ASICs in drift chambers of a few centimeters drift distance [12]–[14]. While already after a few centimeters of drift, the spatial resolution of TPCs is limited by diffusion of the drifting electrons, this approach has the potential to provide superior double-track resolution and measurement of the specific energy loss by cluster counting along with robust pattern recognition in large TPCs.

A 26-cm-long TPC with a triple GEM stack and a single Timepix chip to collect the charge has been introduced in [15] and [16]. After significantly improving the reconstruction and analysis algorithms, we are now able to present a detailed description and analysis of both the apparatus and the recorded data.

This paper is organized as follows. In Section II, the experimental setup is described. The main properties of the Timepix chip are summarized in Section III, and the analysis software is explained in Section IV. The analysis of 27 consecutive days of data-taking with cosmic rays is presented in Section V. Results of the spatial resolution achieved are detailed in Section VI before providing a summary and an outlook in Sections VII and VIII.

II. Experimental Setup

A 26-cm drift length TPC has been set up in Bonn, Germany, to be operated with a triple GEM stack and a single Timepix chip in a cosmic ray test stand (Fig. 1). The readout is triggered by coincident signals of scintillators placed above and below the TPC. Fig. 2 depicts a representative event that has been recorded with this setup.

The TPC drift cylinder with 23 cm inner diameter was designed and constructed at the RWTH Aachen, Aachen, Germany [17]. The aramid honeycomb sandwich structure has a material budget of 1% of a radiation length. The drift field of up to 1 kV/cm is shaped by 187 copper rings that constitute the

Manuscript received June 26, 2012; revised September 10, 2012; accepted September 16, 2012. Date of publication November 21, 2012; date of current version December 11, 2012. This work was supported in part by the European Union and the German federal ministry of research and education (BMBF).

C. Brezina, K. Desch, J. Kaminski, and T. Krautscheid are with the University of Bonn, Bonn 53121, Germany (e-mail: brezina@physik.uni-bonn.de).

M. Killenberg was with the University of Bonn, Bonn 53121, Germany. He is now with CERN, Geneva 1211, Switzerland.

Color versions of one or more of the figures in this paper are available online at http://ieeexplore.ieee.org.

Digital Object Identifier 10.1109/TNS.2012.2220981

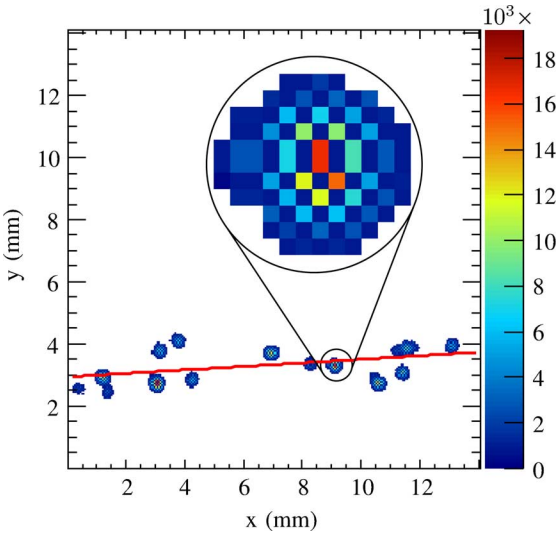

Fig. 2. Display of the full sensitive chip area. The charge depositions detected in a typical event are shown. Depending on the pixel mode, the color code shows either the detected charge or the arrival time of a hit on a pixel (see Section III). A representative pixel cluster is shown in a zoomed view.

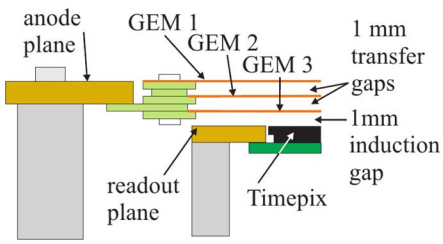

Fig. 3. Schematic drawing of the readout area. The triple GEM stack is embedded in the anode plane. The pixel chip is centered in the readout plane [15], [19].

innermost sandwich layer. These rings are kept at the correct potential by a resistor chain. In our test setup with He:CO_2 (70:30) as drift gas, the drift field was set to 495 V/cm. Thus, an electron drift velocity of 0.974 ± 0.002 cm/μs is expected at 30°C and 1013 mbar from Magboltz [18] simulations.

Both the cathode and the anode are copper planes. The triple GEM stack with the pixel chip readout is embedded into the latter as depicted in Fig. 3. The GEMs have been produced at CERN with 10×10 cm^2 area, 56 μm thickness, and 60–70 μm holes in a hexagonal pattern with 140 μm pitch. The top of GEM 1 is aligned with the anode plane and on the same electrical potential. Therefore, distortions of the drift field are minimized. The transfer gaps and the induction gap are 1 mm each. The voltages across the GEMs are 415 V each, the transfer fields are 2200 V/cm, while the induction field is 3000 V/cm.

Instead of the relatively large readout pads, used in a standard TPC setup, a bare Timepix pixel chip is placed in a central position of the readout plane. The bump-bond pads of the chip, which were originally foreseen to be connected to a silicon sensor, act as charge collecting anodes.

III. Timepix Pixel Chip

The Timepix chip was developed in 2007 by the Medipix2 Collaboration. The chip consists of 256×256 pixels; the pixel size is 55×55 μm^2. A pixel carries a charge-sensitive preamplifier and a single threshold discriminator with a 4-bit adjustment DAC in the analog domain as well as a 14-bit counting logic in the digital part. The digital circuitry may be configured in one of these modes:

- *Single hit:* detect whether the pixel is hit;
- *Medipix:* count the number of events exceeding the threshold level;
- *ToA:* start counting when a pixel is hit and stop with a chip-wide stop signal (shutter). As shown in the timing scheme (Fig. 4), this is a measure of the *T*ime *o*f *A*rrival of the signal;
- *ToT*: count the number of clock cycles that occur while the preamplifier signal is above the threshold. This *T*ime *o*ver *T*hreshold is a direct measure of the charge deposition in the pixel.

The ToA and ToT modes make the Timepix chip well suited for a TPC readout application.

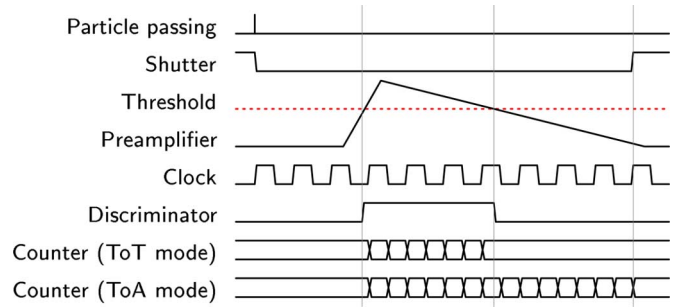

Fig. 4. Timing scheme of the Timepix chip used. The pixels are sensitive when the shutter signal is low. The ToA measurement stops when the shutter is high again. Thus, the point in time when the discriminator detects a hit may be calculated from the ToA counter value and the shutter length. The ToT value is a direct measure of the charge deposition.

Transverse diffusion in the transfer and induction gaps of the GEM stack results in several neighboring pixels being activated by the charge cloud arising from a primary electron. This fact is employed to sample both the arrival time and the charge deposition of a primary electron simultaneously by configuring the pixels in a checkerboard pattern in ToA and ToT modes. Since several (up to 100) pixels are hit by the charge cloud caused by a primary electron, the gain in the GEM stack has to be relatively large, although pixel noise and threshold are low.

The Timepix chip is operated at 55 MHz and read out by a MUROS 2.1 device [20]. The data acquisition software Pixelman [21] is used.

A. Timepix Calibration

An injection capacitor in every pixel on the chip allows a well-defined amount of charge to be deposited in the pixels by applying voltage pulses. This is used to derive a calibration curve converting ToT counts into the input charge in elementary charges. Details on the calibration procedure may be found in [22]. The pixel threshold is determined to be well below 1000 e in our setup.

A similar procedure is used to compensate for the time-walk effect. A test pulse of increasing charge is sent at a fixed time after the shutter signal. The measured ToA of all pixels follows

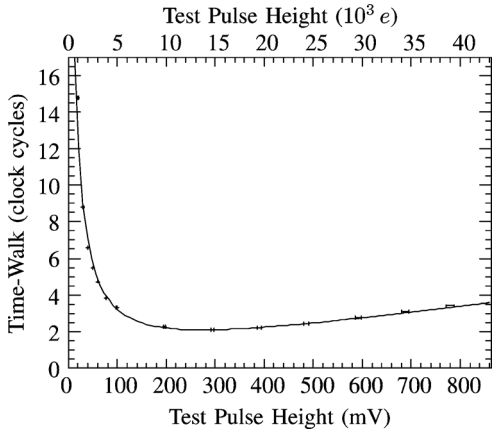

Fig. 5. Time-walk effect as a function of the input charge. Data points are averaged over all pixels of the chip. The rise for test charges above 15 000 electrons can be explained by a shifted working point of the preamplifier. The data are approximated by (1).

a Gaussian distribution. The mean of this distribution depends on the test pulse height and can be interpreted as time-walk TW. The data points as a function of the test pulse charge, Q, (Fig. 5) are described by

$$\mathrm{TW}(Q) = \frac{a}{(Q+b)} + mQ \tag{1}$$

with $a = 289.9 \pm 1.3$ clock cycles, $b = 2.7 \pm 0.3$ mV, and $m = 0.00378 \pm 0.00001$ clock cycles/mV as optimized parameters.

The naively expected monotonic decrease of the time-walk effect cannot be seen since the working point of the preamplifier is affected by very large input charges. Thus, the influence of the time-walk effect decreases with rising input charges and starts slightly rising again for very large charges (more than 15 000 electrons).

This compensation for the time-walk effect can only be applied if a charge information is available for a pixel. Since the charge and the arrival time cannot be measured simultaneously in one pixel, the charge on pixels in ToA-mode has to be interpolated from neighboring pixels in ToT-mode.

IV. Analysis Flow in MarlinTPC

The data analysis is based on the MarlinTPC package [23]. This *m*odular *a*nalysis and *r*econstruction framework for the *lin*ear collider consists of several software modules (called processors) that can be adapted to the special needs of any analysis chain. For these studies, some processors had to be developed in order to accommodate the differences between pixel- and pad-based data analysis flow [24].

While the sequence of the reconstruction processors is more or less fixed, the modularity allows to vary the sequence of the analysis processors. The steps taken to derive reconstructed tracks from the pixels hit are as follows.

1) *Calibration:* The measured ToT is converted to the input charge in electrons, and the time-walk effect is compensated for.
2) *Raw cluster finding:* Neighboring pixels hit are identified to form one connected raw cluster.

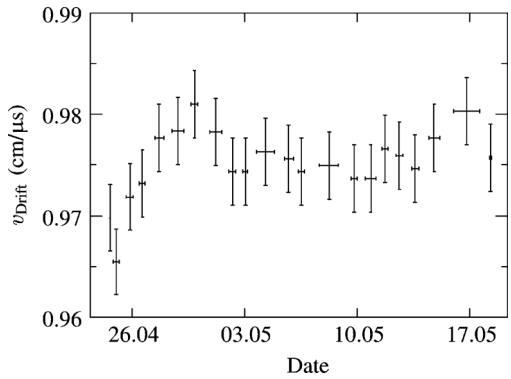

Fig. 6. Measured drift velocity in the drift gas is stable over time within $\pm 0.8\%$ and in perfect agreement with the Magboltz prediction.

3) *Cluster separation:* Detected raw clusters may stem from the superimposed charge clouds of several primary electrons. If possible, these are split into separate pixel clusters as follows.
   First, the principle axis of the raw cluster is determined, and the available charge information is projected onto this axis. Then, if a significant minimum is found in the resulting charge profile, the raw cluster is split at this position.
4) *Hit center calculation:* The original three-dimensional coordinates of a primary ionization are derived from the mean drift time and the center of gravity of all pixels forming a pixel cluster.
5) *Track finding:* All primary electrons forming one track are identified and collected by a two-dimensional Hough transformation in the readout plane.
6) *Track fitting:* A linear regression is used to determine the track parameters.

V. Data Analysis

The maximum drift time of primary electrons in the TPC was used to calculate the drift velocity for each data-taking run during the measurement campaign. The determined mean drift velocity of $\bar{v} = 0.975$ cm/μs is stable within $\pm 0.8\%$ (Fig. 6) and in agreement with Magboltz simulations. This is a good indicator that the overall operation conditions were stable over the three weeks of data-taking.

In order to ensure a good data quality, the analysis has been restricted to single-track events with at least five hits per track. Additionally, a cut on the track angles was applied to make sure that only tracks of cosmic rays are taken into account. Edge effects are eliminated by cuts on the reconstructed position of the primary electrons in the x- and y-directions.

A. Pixel Cluster Characteristics

The most relevant characteristics of the pixel clusters on the Timepix chip are size and charge. Their dependence on the drift distance is shown in Figs. 7 and 8. It can be seen that pixel clusters get smaller for long drift distances until a limit is reached asymptotically. This behavior may be explained by the *declustering effect*.

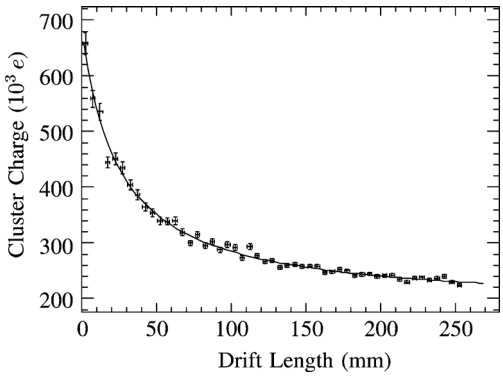

Fig. 7. Due to the declustering effect, the number of detected electrons per pixel cluster is dependent on the drift distance. Fitting (2) to the measured data yields $a = 12530 \pm 560$ e·cm, $b = 25 \pm 2$ cm, and $c = 185 \pm 2\,e$ with $\chi^2/\mathrm{ndf} = 1.8$.

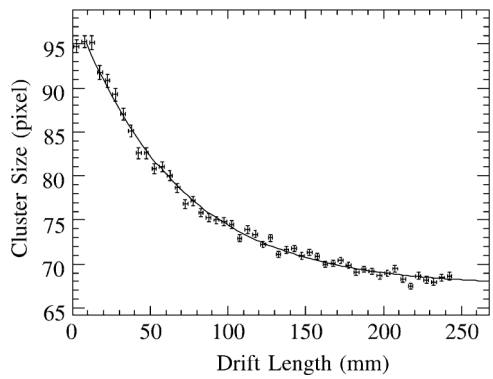

Fig. 8. Dimensions of a pixel cluster are dependent on the drift distance due to the declustering effect. The measured data are well described ($\chi^2/\mathrm{ndf} = 1.7$) by the exponential function (3), with $a = 31.7 \pm 0.6$ pixel, $b = -0.152 \pm 0.005$ cm^{-1}, and $c = 67.5 \pm 0.1$ pixel as parameters.

- Particles passing the TPC volume have a probability to create primary multi-electron clusters in the gas. If the electrons of these primary clusters drift only a short distance until they reach the GEM stack, they will not diffuse apart from each other. Therefore, their individual charge depositions will overlap. Thus, the dimensions and total detected charge of the pixel clusters are larger than expected for a single primary electron.
- With longer drift distances, it becomes more likely that primary multi-electron clusters diffuse apart and each primary electron is detected separately. Therefore, size and charge of a pixel cluster become smaller.

Following this reasoning, the limit in Fig. 7 can be identified with the mean number of electrons originating from one single primary electron. Fitting the empirically found function

$$Q(z) = \frac{a}{b+z} + c \tag{2}$$

to the data results in a lower estimate for the overall gas gain in the triple GEM stack of $c \approx 1.85 \cdot 10^5$. However, one has to keep in mind that the real gain will be larger as some electrons are distributed on pixels that did not pass the threshold level.

B. Simulation of the GEM Stack

In general, it is technically possible to simulate the gas gain of a complete triple GEM stack. However, it is not advisable for large gas gains as in this setup since the computing time is several days per single electron event. To overcome this limitation, the gain of each GEM is calculated separately using ANSYS, for the configuration of the electric field, and Garfield++ [25], for the drift of the electrons. The parameters of the Pólya-distributed gas gain of each GEM are then used to calculate electron avalanches in the GEM stack based purely on statistical considerations such as the active GEM hole area and the diffusion in the transfer- and induction fields. As shown in [26] and [27], one has to keep in mind that the gas gain of a GEM stack is not the exact product of the single GEM gains. Therefore, gain correction factors are applied to the Pólya-distributions. These correction factors are tuned such that the measured total gain is reproduced correctly.

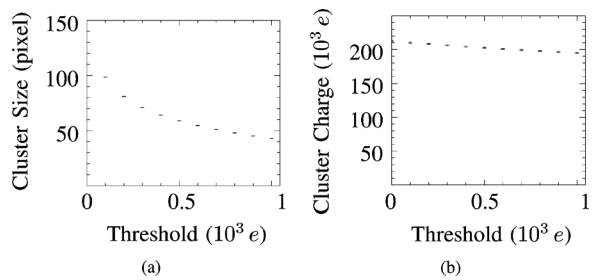

Fig. 9. Simulated dependency of (a) the mean cluster size and (b) the detected charge on the set threshold. Doubling the threshold from 500 to 1000 e reduces the mean size of a charge deposition by roughly 30%, while the total detected charge remains virtually unaffected.

The described algorithm can be used to simulate, for instance, the size of pixel clusters caused by single primary electrons. The latter should be identical to the number of pixels in a cluster originating from real primary electrons with extreme drift distances. In this case, all primary electrons should have drifted apart from each other, and virtually no pixel cluster caused by more than one primary electron is expected. Empirically, it has been found that the measured data shown in Fig. 8 are best described by an exponential decay

$$f(z) = ae^{bz} + c. \tag{3}$$

χ^2-optimization of the free parameters yields the size of a charge deposition in the limit of extreme drift distances: $c = 67.5 \pm 0.1$ pixel, which is compatible with the simulation result of 67.6 ± 0.1 pixel.

Intentional misalignment of the GEMs in the simulation showed no influence on size or summed charge of the individual pixel clusters. Furthermore, the reconstructed position of the primary electron is not dependent on the position of the holes in the lower two GEMs, but only on the position of the top GEM holes, cf. Section VI. The simulation has also been used to determine the dependencies of the pixel clusters caused by single primary electrons on the pixel threshold. From Fig. 9(a) and (b) (size and charge of a deposition), it can be deduced that a remaining threshold dispersion of only a few 100 electrons has an acceptably small effect.

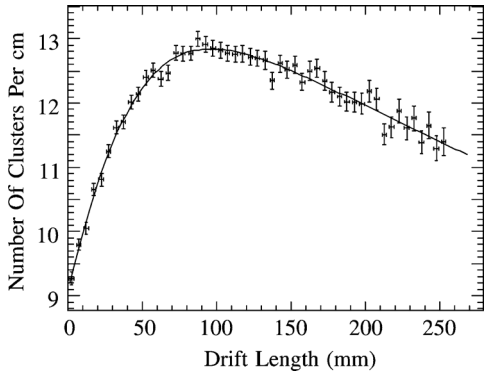

Fig. 10. Number of detected pixel clusters varies with the drift distance. The rise is explained by the declustering effect, while the drop is induced by electron attachment to O_2 molecules. These effects are reproduced with (6).

Equations (2) and (3) describe the z-dependency of charge and size of charge depositions originating from simulated particle tracks with a χ^2/ndf close to 1.

C. Ionization Density

The measured number of pixel clusters per centimeter track length is strongly dependent on the drift distance, just as the bare properties of the detected charge deposition are. This is shown in Fig. 10. The rise in the first centimeters of drift is again explained by the declustering effect: The farther the primary electrons have drifted, the more likely it is that separate pixel clusters are detected. Secondary, the probability for an electron to get attached to molecular O_2 rises with the drift distance. This is the reason for the drop at large drift distances.

The attachment of primary electrons is described by:

$$n_{\mathrm{att}}(z) = Ae^{Bz}. \tag{4}$$

The factor A can be identified with the number of pixel clusters that would be detected if all clusters could be separated and no attachment would happen. The exponential slope B is the attachment rate.

From (3), one can derive the number of primary electrons per charge deposition in dependence on the drift distance

$$n_{\mathrm{electrons/hit}}(z) = 1 + Ce^{Dz} \tag{5}$$

where $(1 + C)$ is the number of primary electrons per pixel cluster after zero drift and D is determined by the separation power of the separation algorithm and the transverse diffusion coefficient.

The overall number of detected pixel clusters per centimeter track length $N(z)$ is therefore described by

$$N(z) = \frac{A}{1 + Ce^{Dz}} \cdot e^{Bz}. \tag{6}$$

A χ^2-optimization of the free parameters yields $A = 14.6 \pm 0.1\ \mathrm{cm}^{-1}$, $B = -0.0099 \pm 0.0004\ \mathrm{cm}^{-1}$, $C = 0.61 \pm 0.02$, and $D = -0.30 \pm 0.03\ \mathrm{cm}^{-1}$ with $\chi^2/\mathrm{ndf} = 0.7$. According to Magboltz simulations, the measured attachment rate B corresponds to approximately 10 ppm oxygen in the drift gas. Since an oxygen absorber was used in the gas stream, this value is plausible. A direct measurement of the oxygen content is not available.

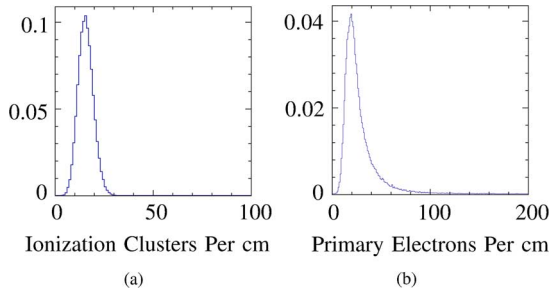

Fig. 11. HEED simulations for (a) the number of collisions per centimeter and (b) the total number of primary electrons per centimeter. Both calculated for incident muons with $\mathrm{p} = 4$ GeV/c in He/CO_2 (70:30).

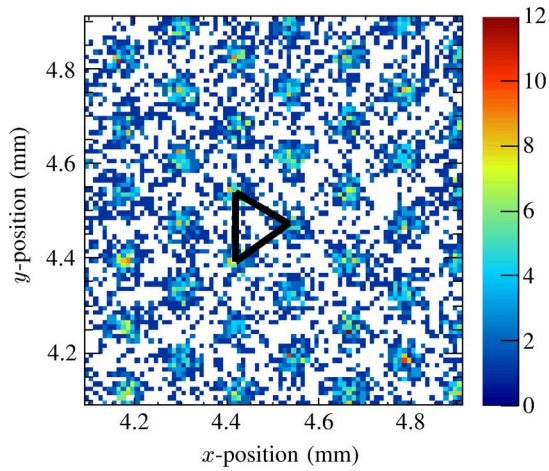

Fig. 12. Zoom of the readout plane, showing the reconstructed centers of the pixel clusters. The pattern of the top GEM is resolved by the pixelized readout. The side length of the drawn triangle is exactly the pitch of the GEM holes (140 μm).

Based on HEED [28] simulations, shown in Fig. 11, one expects roughly 15 primary ionization clusters per centimeter track length in the drift gas originating from incident cosmic muons with $p \geq 4$ GeV/c. In total, this results in 28 primary electrons per centimeter. It is clearly visible that the number of detected charge depositions is significantly lower than the total number of expected primary electrons, while it matches the number of expected ionization points in the gas.

Contrary to the HEED simulation algorithm, primary ionizations caused by high energetic δ-electrons are not associated with the primary particle track by the reconstruction algorithm, but they are identified as separate particle tracks. Thus, the observed number of primary electrons per centimeter tracklength is lower than expected from HEED simulations.

VI. Detector Resolution

Fig. 12 shows the reconstructed center of each pixel cluster of one data acquisition run in a zoom of the occupancy plot. The same regular pattern is seen in simulated data. The distance between two peaks in the histogram is 140 μm, which is exactly the pitch between the holes in the GEMs. Simulations show that each peak is positioned directly underneath a hole in the top GEM. This indicates that the intrinsic transverse single-point

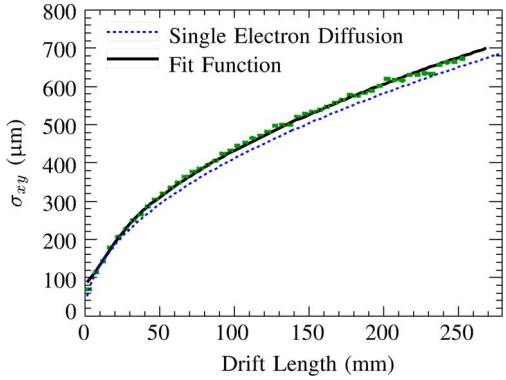

Fig. 13. Observed transverse spatial resolution is close to the theoretical limit given by the single electron diffusion.

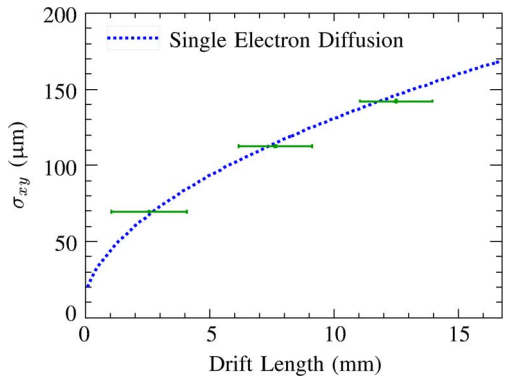

Fig. 14. Extrapolating the data points for small drift distances down to zero drift distance shows that the intrinsic detector resolution is: $\sigma_{0,\mathrm{t}} \leq 50\ \mu$m.

resolution of the prototype TPC is limited by the resolution of the top GEM.

A. Single-Point Resolution

The spatial resolution, σ, is defined as the mean distance of a reconstructed hit to the corresponding reference track. If no data from a beam hodoscope are available for the reference track, the spatial resolution can be derived using the geometric mean method [29]

$$\sigma_{\mathrm{Geo}} = \sqrt{\sigma_N \cdot \sigma_{N-1}} \tag{7}$$

where σ_N is the mean distance of a hit to a track fitted to all hits on the track, and σ_{N-1} is the mean distance of a hit to a track fitted to all hits on the track except the one under investigation.

The spatial resolution for a single primary electron is limited by the diffusion, $D(z)$, of the electron during the drift through the gas volume as follows:

$$D(z) = D_i\sqrt{z} \tag{8}$$

where D_i is either the transverse (D_{t}) or the longitudinal (D_{l}) diffusion coefficient. As long as single electrons are reconstructed, the accuracy of the hit reconstruction can never be better than this limit. TPCs with a standard pad readout detect several primary electrons as one charge deposition. Therefore, the spatial resolution seems to be below this limit. The price that is paid for this virtual performance gain is a loss of hits per track length, which could degrade the accuracy of the track reconstruction.

B. Transverse Spatial Resolution in Dependence on the Drift Distance

As shown in Section V-C it is claimed that the operated TPC prototype is able to detect primary ionization clusters as separate pixel clusters. Roughly 80% of these consist of single primary electrons. Therefore, the spatial resolution is limited by the single electron diffusion as shown in Fig. 13:

All data points are close to the dashed line that represents the single electron diffusion limit for the expected transverse diffusion constant of $D_{\mathrm{t,theo}} = 130 \pm 6\ \mu\mathrm{m}/\sqrt{\mathrm{cm}}$. However, for small drift distances, it was mentioned that some detected charge depositions stem from more than one primary electron.

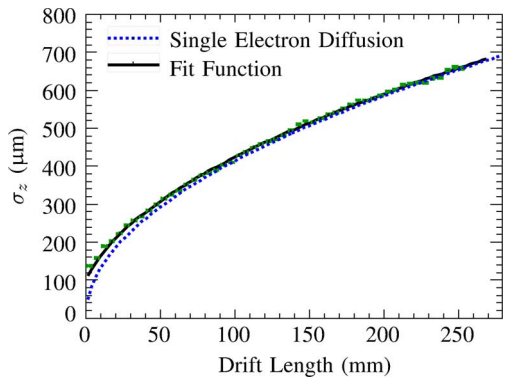

Fig. 15. Observed longitudinal spatial resolution is close to the theoretical limit given by the single electron diffusion.

The applied fit function $\sigma_{xy}(z)$, motivated in [15], takes this into account by introducing an additional factor that rebuilds the number of primary electrons per charge deposition

$$\sigma_{\mathrm{xy}}(z) = \sqrt{\sigma_{0,\mathrm{t}}^2 + \frac{D_{\mathrm{t}}^2 z}{1 + ae^{bz}}}. \tag{9}$$

Usually, TPCs are operated in high magnetic fields and special gas mixtures with small diffusion coefficients. In these scenarios, the resolution is not in general limited by the diffusion, but by the intrinsic detector resolution in the transverse direction, $\sigma_{0,\mathrm{t}}$. This detector parameter can be directly extracted from the data presented in Fig. 14. Here, the transverse spatial resolution is depicted for small drift distances. If one extrapolates the data points down to zero drift distance, it can be seen that the intrinsic transverse detector resolution, $\sigma_{0,\mathrm{t}}$, is indeed limited by the GEM resolution, as already claimed based on Fig. 12.

C. Longitudinal Spatial Resolution Dependence on the Drift Distance

Following the same arguments as for the transverse spatial resolution, one expects that the longitudinal spatial resolution is limited by the single electron diffusion as well. The data presented in Fig. 15 show that this assumption holds in general. The data points are close to the expected diffusion limit $(D_{\mathrm{l,theo}} = 131 \pm 8\ \mu\mathrm{m}/\sqrt{\mathrm{cm}})$, which is depicted by the dashed line.

However, contrary to the transverse resolution, the longitudinal resolution does not benefit from nonseparated primary electrons for small drift distances. This is the case since the Timepix ASIC has no multihit capability. Only the first time, when the threshold in a pixel is passed, is measured. Therefore, in the z-direction, the resolution is slightly degraded for small drift distances.

As explained above, no dependence of the longitudinal resolution on the number of primary electrons per pixel cluster is expected. Thus, a different fit function than for the transverse resolution has to be used

$$\sigma_z = \sqrt{\sigma_{0,l}^2 + D_l^2 z} \tag{10}$$

where D_l is the longitudinal diffusion and $\sigma_{0,l}$ the intrinsic detector resolution in the longitudinal direction.

The limit for the intrinsic resolution in z-direction is not only given by the time resolution of the readout chip (55 MHz corresponds to 18 ns, respectively 175 μm drift per timing bin), but also by effects like a jitter on the shutter window and the remaining time-walk after the time-walk correction is applied as described in Section III-A.

VII. Summary

A TPC prototype with a maximal drift distance of 26 cm was successfully operated with a triple GEM stack for gas amplification and a bare Timepix chip as charge collecting anode. Data taken with He:CO_2 (70:30) as drift gas were presented.

The ASIC has been calibrated, and the time-walk effect was corrected. The properties of the detected charge depositions and the detected ionization density are well understood and in agreement with simulations.

The readout chip resolves the pattern of the gas amplification stage showing the enormous potential of the readout of gaseous detectors with pixel chips. Furthermore, the achieved transverse and longitudinal resolution is at the theoretical limit given by the single electron diffusion during drift.

VIII. Outlook

As long as the pattern of the first GEM is resolved by the readout chip, the resolution is limited by the GEM and not the readout chip. Therefore, the pixel size may be increased without any performance loss.

Such chips have been created by means of wafer post-processing of Timepix wafers at IZM (Berlin, Germany). These modified ASICs carry an additional metallized top layer that combines the area of several pixels. The newly formed bigger pixels are connected to one of the covered original pixels; the others are left floating. The performance of the resulting chips with new pixel sizes of 110×110, 165×165, 220×220, 275×275, 550×550, 55×165, and 55×275 μm^2 is currently being investigated. Additionally, the optimal pixel size may be determined using the above-mentioned simulation algorithm.

Alternatively, GEMs with a finer hole pitch could be used in the GEM stack. However, the charge cloud caused by the primary electrons will still spread out over several pixels, just as in the presented setup. Thus, this option would not relax the demands on the gas gain. The latter should be as small as possible in order to minimize the size of the pixel clusters and to achieve a good double-track resolution in a final application. Furthermore, a smaller gas gain would reduce the undesirable effect of back-drifting ions and prevent aging effects.

Another possibility to achieve an even better matching between gas amplification and readout is to reduce the pitch in the gas amplification stage. This approach is investigated also by means of wafer-post processing. Following a concept developed at NIKHEF, a Micromegas structure with the same pitch as the pixel chip is placed perfectly aligned on the chip. Using such an InGrid (*in*tegrated *grid*) [30], an even better transverse position resolution than with GEMs and pixel readout may be reached. However, such devices are right now not advanced enough to be operated in large TPC applications.

Acknowledgment

The authors would like to thank H. Schindler from CERN for his irreplaceable support on Garfield++ and associated tools. Special thanks go to I. Brock for final proofreading, as well as to C. Krieger and F. Müller for fruitful discussions during data analysis. Furthermore, the support given by NIKHEF and IEAP of the Czech TUP was highly appreciated.

References

[1] D. Nygren, "A time projection chamber," in *Proc. 1975 Pep Summer Study Berkeley*, 1975, no. PEP-0198, pp. 126–133.

[2] Y. Giomataris, P. Rebourgeard, J. Robert, and G. Charpak, "Micromegas: A high-granularity position-sensitive gaseous detector for high particle-flux environments," *Nucl. Instrum. Methods A*, vol. 376, no. 1, pp. 29–35, 1996.

[3] N. Abgrall *et al.*, "Time projection chambers for the T2K near detectors," *Nucl. Instrum. Methods A*, vol. 637, no. 1, pp. 25–46, 2011.

[4] F. Sauli, "GEM: A new concept for electron amplification in gas detectors," *Nucl. Instrum. Methods A*, vol. 386, no. 2–3, pp. 531–534, 1997.

[5] The ILD Concept Group, "The International Large Detector: Letter of intent," 2010.

[6] J. Brau, Ed. *et al.*, "ILC reference design report: ILC global design effort and world wide study," 2007.

[7] P. Schade and J. Kaminski, "A large TPC prototype for a linear collider detector," *Nucl. Instrum. Methods A*, vol. 628, no. 1, pp. 128–132, 2011.

[8] R. Bellazzini, F. Angelini, L. Baldini, F. Bitti, A. Brez, M. Ceccanti, L. Latronico, M. M. Massai, M. Minuti, N. Omodel, M. Razzano, C. Sgrò, G. Spandre, E. Costa, and P. Soffitta, "Reading a GEM with a VLSI pixel ASIC used as a direct charge collecting anode," *Nucl. Instrum. Methods A*, vol. 535, no. 1–2, pp. 477–484, 2004.

[9] R. Bellazzini, F. Angelini, L. Baldini, F. Bitti, A. Brez, F. Cavalca, M. Del Prete, M. Kuss, L. Latronico, N. Omodel, M. Pinchera, M. M. Massai, M. Minuti, M. Razzano, C. Sgrò, G. Spandre, A. Tenze, E. Costa, and P. Soffitta, "Gas pixel detectors for X-ray polarimetry applications," *Nucl. Instrum. Methods A*, vol. 560, no. 2, pp. 425–434, 2006.

[10] X. Llopart, M. Campbell, R. Dinapoli, D. San Segundo, and E. Pernigotti, "Medipix2: A 64-k pixel readout chip with 55 μm square elements working in single photon counting mode," *IEEE Trans. Nucl. Sci.*, vol. 49, no. 5, pp. 2279–2283, Oct. 2002.

[11] X. Llopart, R. Ballabriga, M. Campbell, L. Tlustos, and W. Wong, "Timepix, a 65 k programmable pixel readout chip for arrival time, energy and/or photon counting measurements," *Nucl. Instrum. Methods A*, vol. 581, no. 1–2, pp. 485–194, 2007.

[12] A. Bamberger, K. Desch, U. Renz, M. Titov, N. Vlasov, P. Wienemann, and A. Zwerger, "Triple-GEM operated in different gases with highly pixelated readout using MediPix2 chip," *Nucl. Instrum. Methods A*, vol. 572, no. 1, pp. 157–159, 2007.

[13] A. Bamberger, K. Desch, U. Renz, M. Titov, N. Vlasov, P. Wienemann, and A. Zwerger, "Resolution studies on 5 GeV electron tracks observed with triple-GEM and MediPix2/TimePix-readout," *Nucl. Instrum. Methods A*, vol. 581, no. 1–2, pp. 274–278, 2007.

[14] A. Bamberger, K. Desch, U. Renz, M. Titov, N. Vlasov, P. Wienemann, and A. Zwerger, "Readout of GEM detectors using the Medipix2 CMOS pixel chip," *Nucl. Instrum. Methods A*, vol. 573, no. 3, pp. 361–370, 2007.
[15] C. Brezina, K. Desch, J. Kaminski, M. Killenberg, F. Klöckner, T. Krautscheid, U. Renz, and M. Schumacher, "A time projection chamber with triple gem and pixel readout," *J. Instrum.*, vol. 4, no. 11, p. P11015, 2009.
[16] I. Kaminski, C. Brezina, K. Desch, M. Killenberg, T. Krautscheid, C. Krieger, F. Müller, and M. Schultens, "Gaseous detectors with micropattern gas amplification stages and CMOS pixel chip readout," *J. Instrum.*, vol. 7, no. 02, p. C02035, 2012.
[17] S. Blatt, "Konstruktion und Inbetriebnahme eines Feldkäfigs für eine TPC," 2004.
[18] S. Biagi, "Magboltz," CERN, 2010.
[19] L. Kaminski, M. Killenberg, A. Bamberger, H. Blank, C. Brezina, K. Desch, T. Krautscheid, W. Ockenfels, U. Renz, M. Ummenhofer, P. Wienemann, S. Zimmermann, and A. Zwerger, "Time projection chamber with triple gem and pixel readout," in *IEEE NSS Conf. Rec.*, Oct. 2008, pp. 2926–2929.
[20] D. S. S. Bello, M. van Beuzekom, P. Jansweijer, H. Verkooijen, and J. Visschers, "An interface board for the control and data acquisition of the Medipix2 chip," *Nucl. Instrum. Methods A*, vol. 509, no. 1–3, pp. 164–170, 2003.
[21] T. Holy, J. Jakubek, S. Pospisil, J. Uher, D. Vavrik, and Z. Vykydal, "Data acquisition and processing software package for Medipix2," *Nucl. Instrum. Methods A*, vol. 563, no. 1, pp. 254–258, 2006.
[22] L. Jakubek, "Precise energy calibration of pixel detector working in time-over-threshold mode," *Nucl. Instrum. Methods A*, vol. 633, pp. S262–S266, 2011.
[23] J. Abernathy, K. Dehmelt, R. Diener, J. Engels, J. Hunt, M. Killenberg, T. Krautscheid, A. Munnich, S. Zimmerman, M. Ummenhofer, A. Vogel, and P. Wienemann, "MarlinTPC: A common software framework for TPC development," in *IEEE NSS Conf. Rec.*, Oct. 2008, pp. 1704–1708.
[24] S. Zimmermann, "Data reconstruction and analysis of GEM—Based time projection chambers with pixel readout," 2008.
[25] H. Schindler and R. Veenhof, "Garfield++," CERN, 2011.
[26] S. Bachmann, A. Bressan, L. Ropelewski, F. Sauli, A. Sharma, and D. Mörmann, "Charge amplification and transfer processes in the gas electron multiplier," *Nucl. Instrum. Methods A*, vol. 438, no. 2–3, pp. 376–408, 1999.
[27] F. Sauli, "Development and applications of gas electron multiplier detectors," *Nucl. Instrum. Methods A*, vol. 505, no. 1–2, pp. 195–198, 2003.
[28] I. Smirnov, "Modeling of ionization produced by fast charged particles in gases," *Nucl. Instrum. Methods A*, vol. 554, no. 1–3, pp. 474–493, 2005.
[29] S. Biagi, "Monte Carlo simulation of electron drift and diffusion in counting gases under the influence of electric and magnetic fields," *Nucl. Instrum. Methods A*, vol. 421, no. 1–2, pp. 234–240, 1999.
[30] M. Chefdeville, P. Colas, Y. Giomataris, H. van der Graaf, E. Heijne, S. van der Putten, C. Salm, J. Schmitz, S. Smits, J. Timmermans, and J. Visschers, "An electron-multiplying Micromegas grid made in silicon wafer post-processing technology," *Nucl. Instrum. Methods A*, vol. 556, no. 2, pp. 490–494, 2006.